Available online at www.sciencedirect.com
ScienceDirect
Polymer 48 (2007) 3286–3293
polymer
www.elsevier.com/locate/polymer

Deformation behaviour during cold drawing of nanocomposites based on single wall carbon nanotubes and poly(ether ester) copolymers

J.J. Hernández [a], M.C. García-Gutiérrez [a,*], A. Nogales [a], D.R. Rueda [a], A. Sanz [a], I. Sics [b], B.S. Hsiao [c], Z. Roslaniec [d], G. Broza [e], T.A. Ezquerra [a]

[a] *Instituto de Estructura de la Materia, CSIC, Serrano 121, 28006 Madrid, Spain*
[b] *CELLS – ALBA, 08193 Bellaterra, Barcelona, Spain*
[c] *Department of Chemistry, State University of New York at Stony Brook, NY 11794-3400, USA*
[d] *Szczecin University of Technology, Institute of Materials Science and Engineering, Piastow Av. 19, PL-70310 Szczecin, Poland*
[e] *Technische Universität Hamburg-Harburg, Denickestrasse 15, D-21071 Hamburg, Germany*

Received 5 December 2006; received in revised form 14 March 2007; accepted 24 March 2007
Available online 5 April 2007

Abstract

Relationships between the macroscopic deformation behaviour and microstructure of a pure (PBT-*b*-PTMO) block copolymer and a polymer nanocomposite (PBT-*b*-PTMO + 0.2 wt% SWCNT) were investigated by simultaneous small- and wide-angle X-ray scattering (SAXS and WAXS) during tensile deformation using synchrotron radiation. The Young's modulus was found to be 15% higher for the nanocomposite than for the pure block copolymer as well as the yield strength, while the elongation-to-break was less than a half. This different behaviour can be explained by taking into account the different structural features revealed by SAXS and WAXS and thus considering that SWCNT act as anchors in the nanocomposite, sharing the applied stress with the PBT crystals and partially preventing the flexible, non-crystallisable PTMO chains to elongate.

Keywords: Polymer nanocomposites; Deformation behaviour; Simultaneous SAXS and WAXS

1. Introduction

Thermoplastic elastomers combine high-temperature mechanical strength and low-temperature flexibility [1]. These elastomers are block copolymers which contain alternate crystallisable (hard) and non-crystallisable (soft) chain segments, resulting in a material with high melting temperature crystallites (hard component) dispersed in a soft, low glass transition temperature matrix. Segmented poly(ether ester) copolymers of PBT and PTMO belong to the family of such thermoplastic elastomers [2]. The nanometric structure of segregated hard and soft segments is mainly responsible for the mechanical properties of these polymers [2,3]. On the other hand, single wall carbon nanotubes (SWCNT) with a diameter of 0.6–1.8 nm and a length of several microns exhibit a Young's modulus of about 1.25 TPa [4] (100 times stronger than steel with six times lower density) and higher electrical and thermal conductivity than copper. This makes SWCNT ideal as the reinforcing elements in nanocomposite materials, with great potential to improve the polymer properties as a result of physical and chemical interphase interactions [5]. It is known that in order to transfer the outstanding mechanical properties of SWCNT to the composite material the most essential step involves the dispersion of nanotubes within the polymer matrix. There are several works showing that nanotubes are not isolated from the nanocomposite [6–8]. SWCNT are mostly arranged into ropes with a close-packed stacking, which thus form self-assembled cables on the nanometer scale [9,10]. Elastic and shear moduli of SWCNT ropes are in the order

* Corresponding author. Tel.: +34 915616800; fax: +34 915645557.
E-mail address: imtc304@iem.cfmac.csic.es (M.C. García-Gutiérrez).

0032-3861/$ - see front matter © 2007 Elsevier Ltd. All rights reserved.
doi:10.1016/j.polymer.2007.03.070

of 1 TPa and 1 GPa, respectively [11], and the yield strength is about 45 GPa [12] (20 times the yield strength of typical high-strength steels). Elastic modulus and yield strength of SWCNT ropes are excellent, but they have low shear modulus due to poor intertube cohesion.

Few works have been reported about simultaneous SAXS/WAXS studies during deformation of polymer-CNT nanocomposites [13]. The aim of the present study is to establish direct relationships between the macroscopic deformation behaviour and the microstructure of a pure (PBT-*b*-PTMO) block copolymer and a polymer nanocomposite (PBT-*b*-PTMO + 0.2 wt% SWCNT), in order to know the role of SWCNT in the deformation behaviour of this kind of nanocomposites.

2. Experimental section

2.1. Materials and sample preparation

The chosen polymer matrix was a copolymer (PBT-*b*-PTMO) consisting of hard blocks with ester units, poly(butylene terephthalate) (PBT) and soft blocks with ether units, poly(tetramethylene oxide) (PTMO). The content of hard segments based on PBT was 45 wt% and the content of soft segments based on PTMO was 55 wt%. The morphology in this copolymer consisted of semicrystalline PBT domains dispersed in the soft matrix of amorphous, non-crystallisable PTMO [14,15]. The average molecular weight of the copolymer was approximately 26,000 g/mol.

The nanocomposite with 0.2 wt% of SWCNT (MER Corp., Tucson, Arizona, USA) was prepared in situ by introducing the filler into a reaction mixture for synthesis of multiblock poly(ether ester) copolymer (PEE) by polycondensation in the molten state. The SWCNT were dispersed by ultrasonication and high-speed stirring in 1,4-butanediol (BASF, Germany). The synthesis of the multiblock poly(ether ester) copolymer with the dispersed SWCNT was a two-stage process which has been described elsewhere [16]. The resulting materials were extruded from the reactor by compressed nitrogen and then pelletized. Scanning electron microscopy shows good dispersion of nanotubes in the polymer matrix [16].

The samples were put into a mould and melt-pressed at 260 °C under a pressure of 4000 kg/m^2 for 3 min. The molded samples were quenched in ice water. The samples have a dumbbell shape with dimensions of 25 mm length, 7 mm wide and 0.85 mm thick.

2.2. Instrumentation and experimental procedures

In situ time-resolved SAXS (small-angle X-ray scattering) and WAXS (wide-angle X-ray scattering) experiments were performed at the X27C beamline in the National Synchrotron Light Source (NSLS), Brookhaven National Laboratory (BNL), USA. The wavelength of the X-ray beam was monochromatised to 0.1371 nm using a double multilayer Si/W monochromator. The X-ray beam was collimated to 0.4 mm size (at the sample position) using a three pinhole collimation system. Two-dimensional SAXS and WAXS patterns were recorded on two Fuji HR-VTM imaging plates (200 × 250 mm) with sample-detector distances of 1914.4 and 129.5 mm, respectively. The WAXS imaging plate contained a central opening with a diameter of 20 mm to allow the passage of the SAXS signal. A FUJI BAS 2500 imaging plate scanning station was used to digitize the image recorded on the plates. The patterns were digitized at a resolution of 100 μm/pixel. The SAXS scattering angle was calibrated by silver behenate standard while the WAXS scattering angle was calibrated by Al_2O_3 diffraction standard from the National Institute of Standards and Technology (NIST).

Stretching of the sample was accomplished by using a modified Instron 4410 tensile apparatus. The Instron apparatus was mounted in such a way that the centre of the sample was in the beam path. This machine provided symmetric deformation where the same part of the sample remained in the beam path during the stretching. After the sample was mounted and placed into the Instron grips, extension was applied at a crosshead speed of 1 mm/min. The strain at time t was calculated as $100 \times (l - l_0)/l_0$, where l is the length of the sample at time t and l_0 is the original length of the sample. Simultaneous SAXS and WAXS images were recorded using image collection time of 60 s during the deformation experiment. 2D SAXS and WAXS patterns were corrected for the incident beam intensity fluctuations, as well as air and instrument scatterings.

3. Results

Fig. 1 shows the engineering stress–strain curves for the PBT-*b*-PTMO copolymer and for the nanocomposite with 0.2 wt% of SWCNT, obtained during drawing at room temperature. The pictures below represent in situ simultaneous SAXS (top) and WAXS (bottom) patterns collected at selected strains for the copolymer (A) and for the nanocomposite (B). In both cases, copolymer and nanocomposite, the SAXS and WAXS patterns exhibited continuous changes with increasing applied strain, indicating a close correlation between the microstructure and the mechanical properties of the samples.

The stress–strain curve of the PBT-*b*-PTMO copolymer exhibits an initial region of elastic deformation at strains lower than 38%, where the stress increases sharply. In this region, WAXS patterns typical of the undeformed sample are shown, consisting of circular diffraction rings corresponding to the Bragg reflections of the α form PBT crystals [17]. At strains larger than 38%, the stress increases slowly with strain and the Bragg reflections accumulate the intensity along the equator (perpendicular to the stretching direction). The corresponding SAXS patterns show a different evolution trend with the strain. The initial isotropic ring for the undeformed sample becomes gradually anisotropic having an arc on the meridian (stretching direction). In pattern 3 the arc on the meridian splits into two maxima and with increasing strain the arc with two maxima appears to be spread horizontally (pattern 4). With a further increase of strain (patterns 5 and 6), the SAXS intensity shows a strong maximum on the meridian, together with a sharp scattering streak along the equator.

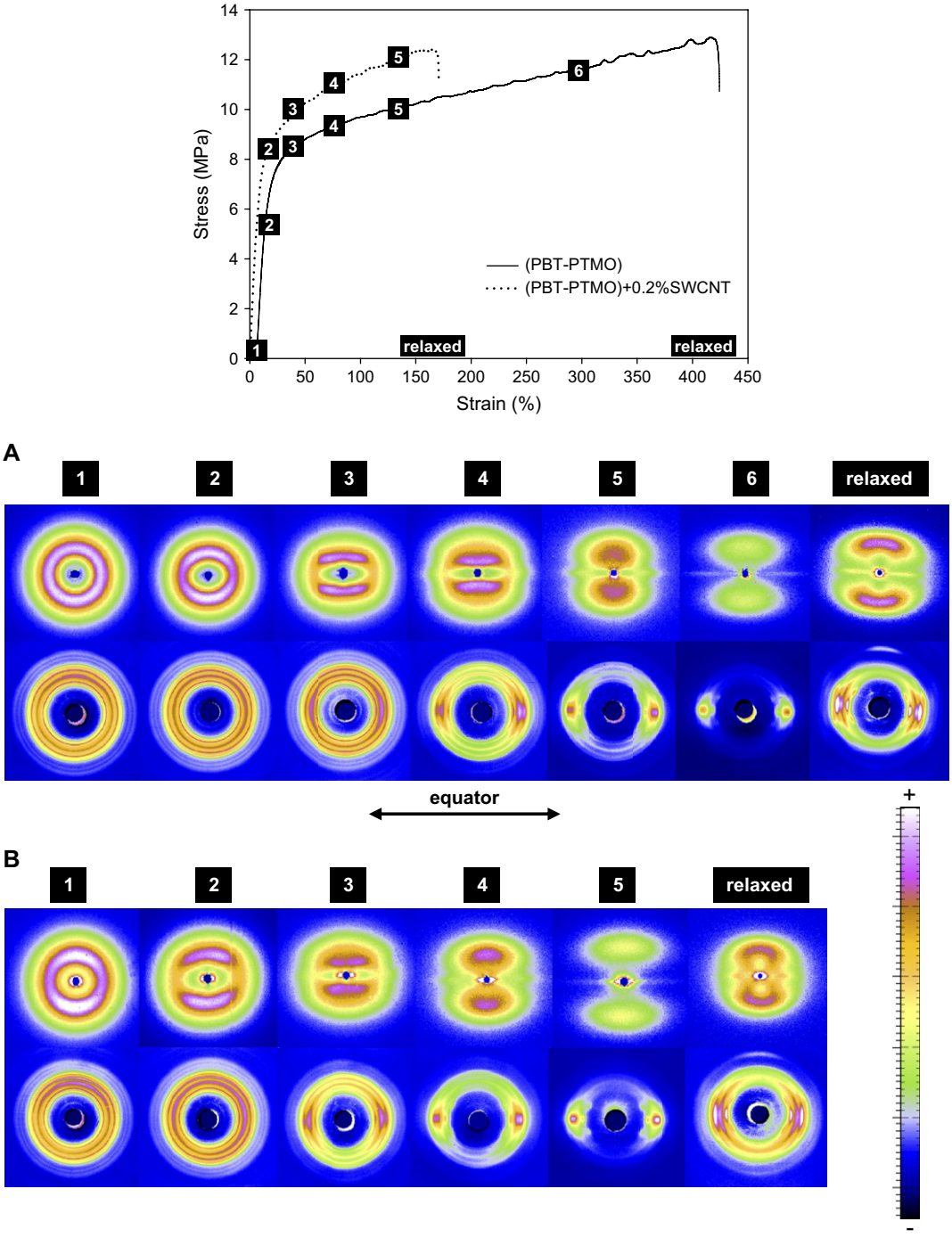

Fig. 1. Stress–strain curves for the PBT-*b*-PTMO block copolymer (solid line) and for the nanocomposite with 0.2 wt% SWCNT (dotted line). The pictures below present in situ simultaneous SAXS (top) and WAXS (bottom) patterns selected at specific values of strain. The panel A corresponds to the copolymer and panel B to the nanocomposite.

The nanocomposite with 0.2% of SWCNT exhibits a stress–strain curve having a region of elastic deformation at strains lower than 25%, showing even a more pronounced increase in the stress than the PBT-*b*-PTMO copolymer. It can be seen that the elongation-to-break for the nanocomposite is less than half the elongation-to-break for the pure block copolymer. However, the stress at break is similar for the two. The evolutions of WAXS and SAXS patterns with increasing strain are similar for nanocomposite and copolymer but at a different time scale. The WAXS and SAXS patterns taken after the break of the samples (patterns named relaxed) show a loss of orientation in both systems due to relaxation of the material. This effect is more prominent for the nanocomposite than for the copolymer.

In order to analyze the positional changes of the SAXS maximum with strain, radial intensity profiles were extracted

from the azimuth integration in the meridian region of the 2D SAXS patterns. At strains higher than 5%, the SAXS patterns show a cylindrical symmetry. In these cases, a projection operation was applied to obtain the integrated intensity on the meridian ($I_1(q_3)$) using the expression

$$I_1(q_3) = \int_0^\infty I(q_{12}, q_3) q_{12}\, \mathrm{d}q_{12} \quad (1)$$

Here, (q_3) is the project direction that corresponds to the meridian direction, and all the intensities in the q_{12} plane, which has the same q_3 value have been projected onto an array member $I_1(q_3)$. In Fig. 2, the meridian intensity profiles are plotted against the scattering vector ($q = 4\pi \sin\theta/\lambda$, λ being the wavelength and 2θ the scattering angle) at different strains. The sets of curves A and B correspond to the copolymer and the nanocomposite, respectively. Fig. 3 shows the variation of the meridian long spacing L ($L = 2\pi/q_m$, q_m being the position of the maxima in Fig. 2), between the crystalline lamellae, with strain for both copolymer (empty circles) and nanocomposite (filled circles). To facilitate the comparison, the stress–strain curves (solid and doted lines, respectively) are superimposed in the same figure. In the initial stage the long spacing increases linearly with strain until the value of $\varepsilon = 61\%$ for copolymer and the value of $\varepsilon = 38\%$ for nanocomposite. For strains higher, the long spacing decreases until values slightly below the initial value for both copolymer and nanocomposite.

As pointed out in the description of Fig. 1, at high strains the SAXS patterns show a scattering streak along the equator. The radial intensity profiles have been extracted from the azimuthal integration of the equatorial region from the 2D SAXS patterns. In Fig. 4, the equatorial intensity profiles are plotted against the scattering vector q only at strains where the SAXS equatorial streak presents a maximum of intensity. The sets of curves A and B correspond to the copolymer and nanocomposite, respectively. It should be noted that in nanocomposite, the maximum appears as a shoulder imposed to a higher continuous scattering due to SWCNT. Fig. 5 shows the variations of the equatorial long spacing L_{eq} ($L_{eq}=2\pi/q_{eq}$, q_{eq} being the position of the maxima in Fig. 4), as a function of strain for both copolymer (empty circles) and nanocomposite (filled circles). It can be seen that the equatorial long spacing increases with strain to a similar value for both samples (the process is much faster for nanocomposite). It should be pointed out

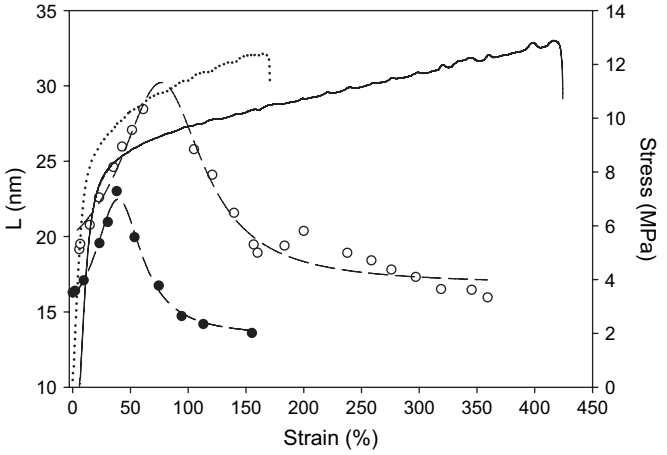

Fig. 3. Meridian long spacing as a function of applied strain as calculated by Bragg's law: for the copolymer (○) and for the nanocomposite (●). For comparison, the stress–strain curves are superimposed. The dashed line is a guide for the eye.

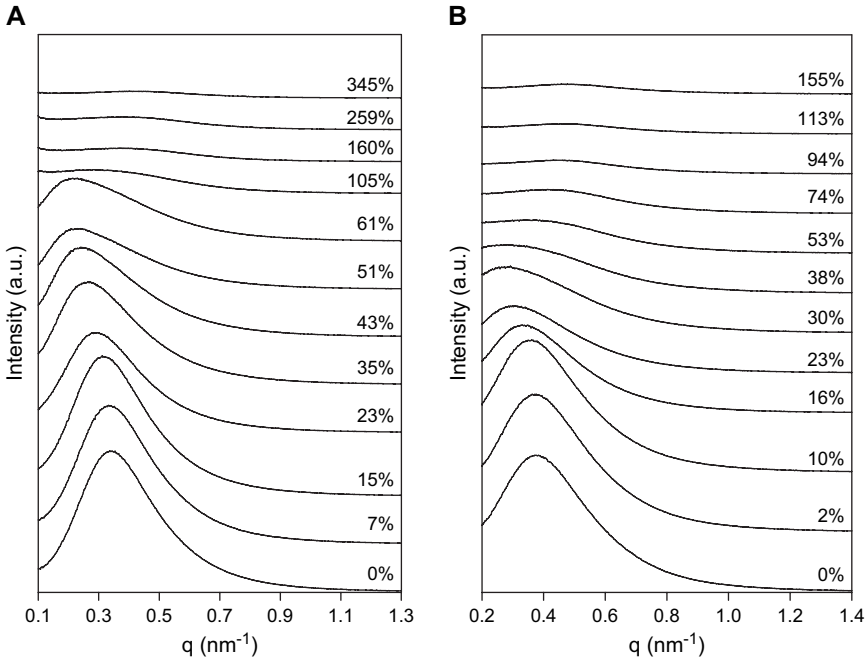

Fig. 2. Meridian intensity profiles extracted from the 2D SAXS patterns for the copolymer (panel A) and the nanocomposite (panel B), measured at indicated strain values. Curves have been vertically shifted for clarity.

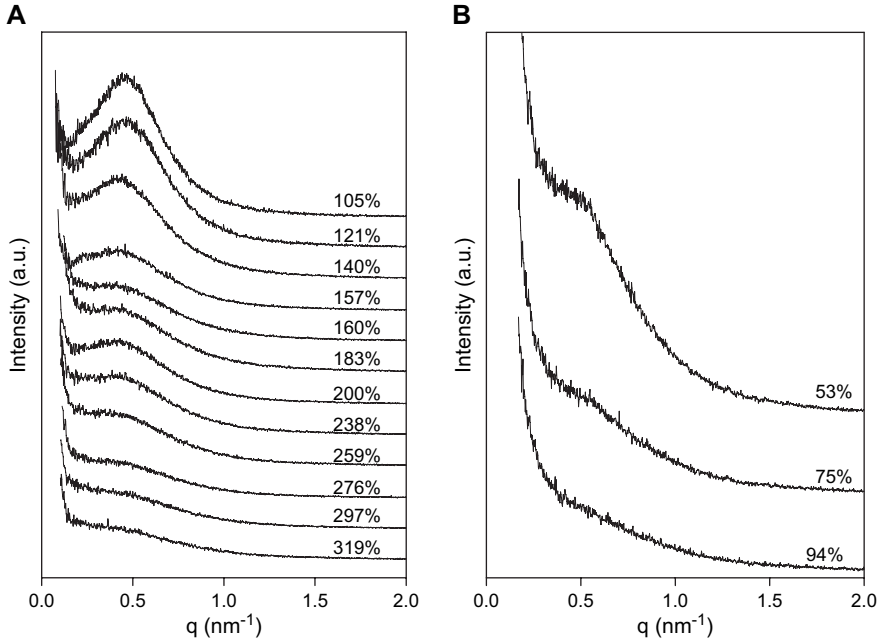

Fig. 4. Equatorial intensity profiles extracted from the 2D SAXS patterns for the copolymer (panel A) and the nanocomposite (panel B), measured at indicated strain values. Curves have been vertically shifted for clarity.

that the equatorial intensity maximum and thus the equatorial long spacing for nanocomposite disappears at strain values larger than 100%, while it remains at strain of 320% for copolymer.

The 2D WAXS patterns were azimuthally integrated, in the whole angular range (0–360°), in order to obtain the radial intensity profiles. These curves were deconvoluted as individual crystalline peaks and the amorphous halo. The degree of crystallinity was calculated from the equation $X_c = \sum I_c / \sum (I_a + I_c)$, where I_c is the integrated area underneath the crystalline peaks and I_a is the integrated area of the amorphous halo. X_c values are illustrated in Fig. 6 as a function of strain. It is seen that the degree of crystallinity is slightly higher for nanocomposite than for copolymer at a given strain. In addition, the degree of crystallinity is almost constant in the region of elastic deformation for both the copolymer and the nanocomposite. At higher strains, the degree of crystallinity decreases with increasing strain.

In order to obtain information about the evolution of crystal perfection with applied strain, the apparent crystallite size (ACS), associated with the 010 reflection was calculated using the Scherrer equation [18]

$$\mathrm{ACS} = \frac{0.9\lambda}{(\Delta 2\theta)\cos\theta} \tag{2}$$

where λ is the X-ray wavelength, $(\Delta 2\theta)$ is the width at half-intensity maximum of the 010 reflection in radians, and θ is

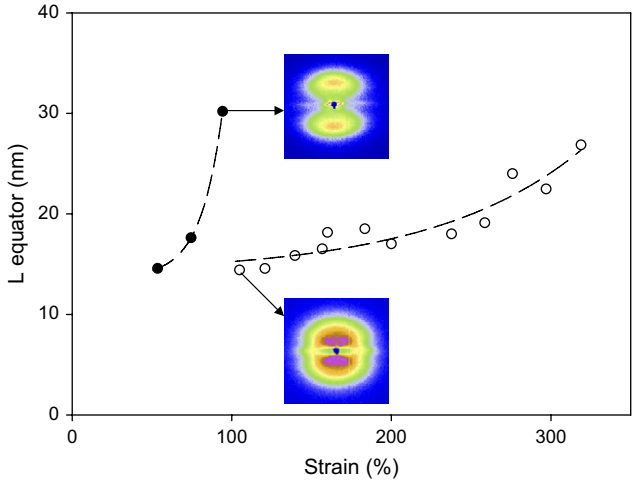

Fig. 5. Equatorial long spacing as a function of applied strain: for the copolymer (○) and for the nanocomposite (●). The first pattern that presents the equatorial maximum in the copolymer and the last one for the nanocomposite are presented. The dashed line is a guide for the eye.

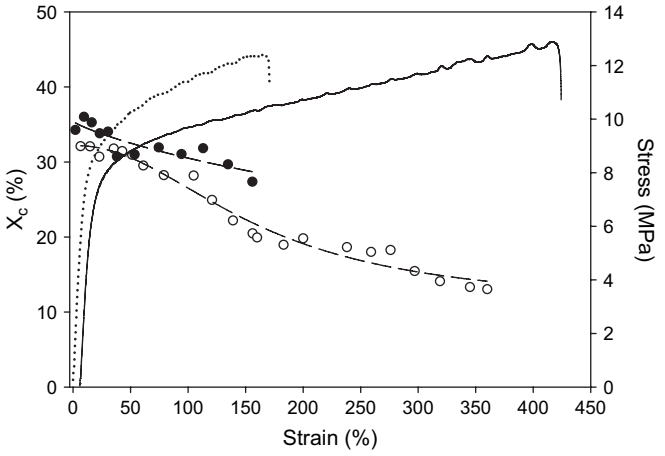

Fig. 6. Degree of crystallinity calculated from the WAXS patterns versus the applied strain: for the copolymer (○) and for the nanocomposite (●). The dashed line is a guide for the eye.

half the scattering angle of the crystalline peak. In order to improve the statistics and to be able to calculate the ACS even at very high strains, the 2D WAXS patterns were azimuthally integrated taking into account a cake centred at the equator (at the 010 reflection) with the following limits: $14^\circ \leq 2\theta \leq 17^\circ$ and $-20^\circ \leq \varphi \leq 20^\circ$. In Fig. 7, the ACS value for both copolymer and nanocomposite is presented as a function of strain. The ACS is slightly larger for the copolymer and decreases with increasing strain for both materials.

4. Discussion

The above results indicate that the application of macroscopic deformation induces considerable changes in microstructure for both block copolymer and nanocomposite. However, there are some differences between them. From the stress–strain curves in Fig. 1, the mechanical behaviour between the PBT-*b*-PTMO block copolymer and the nanocomposite with 0.2 wt% of SWCNT is quite different. We attempt to discuss these differences on the basis of the changes in microstructure that take place during deformation and considering some molecular mechanisms.

4.1. Elastic deformation region

The first difference to point out is that the Young's modulus, calculated from the elastic region in the stress–strain curves, has a value of $E = 75.8$ MPa for the copolymer and $E = 87.6$ MPa for the nanocomposite. Thus, the Young's modulus is about 15% higher in case of nanocomposite. As it has been reported for a similar PBT-*b*-PTMO block copolymer [14,19], the elongation of amorphous chains and the orientation of crystalline domains all increase with strain in the elastic region. As a result, the PBT lamellae tend to be aligned perpendicular to the drawing direction, and both PTMO and PBT chains tend to arrange parallel to the stretching. In the present work, we also have observed evidences to invoke this behaviour for both copolymer and nanocomposite. The isotropic SAXS/WAXS patterns obtained from the initial state of the copolymer (Fig. 1A, pattern 1) indicate a random orientation of the semicrystalline PBT domains in the sample. In contrast, the initial SAXS pattern taken from the nanocomposite (Fig. 1B, pattern 1) indicates that the scattered intensity slightly concentrates on the meridian, indicating a small initial degree of orientation of the semicrystalline PBT domains. This may be due to the templating effect of the carbon nanotubes during processing of the samples [20]. With increasing strain, one observes the distortion of the SAXS patterns of the copolymer from the initial circular shape into an ellipsoidal shape with the scattered intensity concentrated on the meridian (Fig. 1A, pattern 2). This indicates that the crystalline domains reoriented themselves perpendicularly to the stretching direction. As strain increases, the amorphous PTMO chains are elongated while the crystalline PBT chains remain unchanged, resulting in an increase of the separation distance between the PBT crystalline domains. In Fig. 3, one observes an affine relationship between the long spacing and the applied strain for both copolymer and nanocomposite. Nevertheless, the increase of the long spacing with strain is smaller for nanocomposite than for copolymer. This could be explained by assuming that nanotubes act as anchors and partially prevent the flexible, amorphous PTMO chains to elongate. A visualization of these mentioned features can be found in the scheme presented in Fig. 8. Initially the isotropic SAXS pattern of the copolymer (pattern A, left in Fig. 8) indicates a random orientation of the semicrystalline PBT domains in the sample, while the initial SAXS pattern taken from the nanocomposite (pattern A, right) presents the scattered intensity slightly concentrated at the meridian, indicating an initial degree of orientation of the semicrystalline PBT domains due to the templating effect of the carbon nanotubes during processing. Under stress but still in the elastic region, the SAXS signal becomes gradually anisotropic showing an arc on the meridian (patterns B of Fig. 8), indicating the rotation of the crystal lamellae in order to be aligned along the stretching direction.

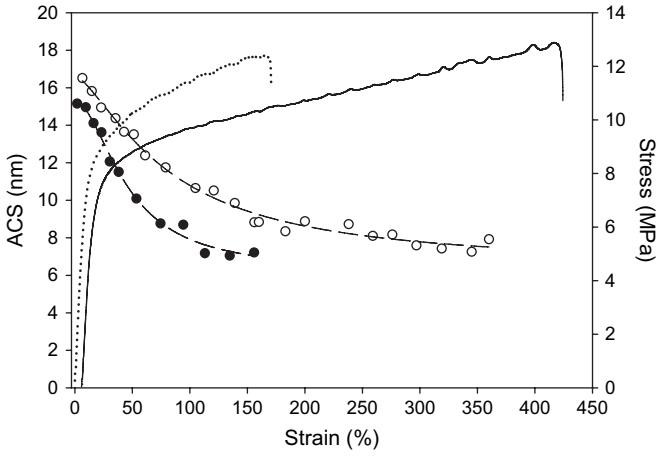

Fig. 7. Apparent crystallite size (ACS) calculated from the 010 reflection as a function of applied strain: for the copolymer (○) and for the nanocomposite (●). The dashed line is a guide for the eye.

4.2. Plastic deformation region

Taking into account the results of Figs. 6 and 7 about the evolution of crystallinity and apparent crystallite size upon the applied strain, it is evident that SWCNT are playing the role of the nucleating agent in the nanocomposite. Thus, while the degree of crystallinity is somewhat larger for the nanocomposite, the PBT crystallite size along the 010 direction is considerably reduced by the presence of SWCNT.

At strains higher than 38% in the copolymer and 25% for nanocomposite, the rate of increase in stress becomes much smaller than that in the elastic region. We can explain this with the behaviour of an irreversible breakage of the PBT crystalline lamellae which, as it has been reported [14,15,19], takes place in different sequential steps. Firstly, the breakage of the initial crystalline lamellae occurs giving rise to a four point SAXS diagram for the copolymer case (Fig. 8C, left). For nanocomposite (Fig. 8C, right), the order of the fragmented lamellae is distorted by the presence of

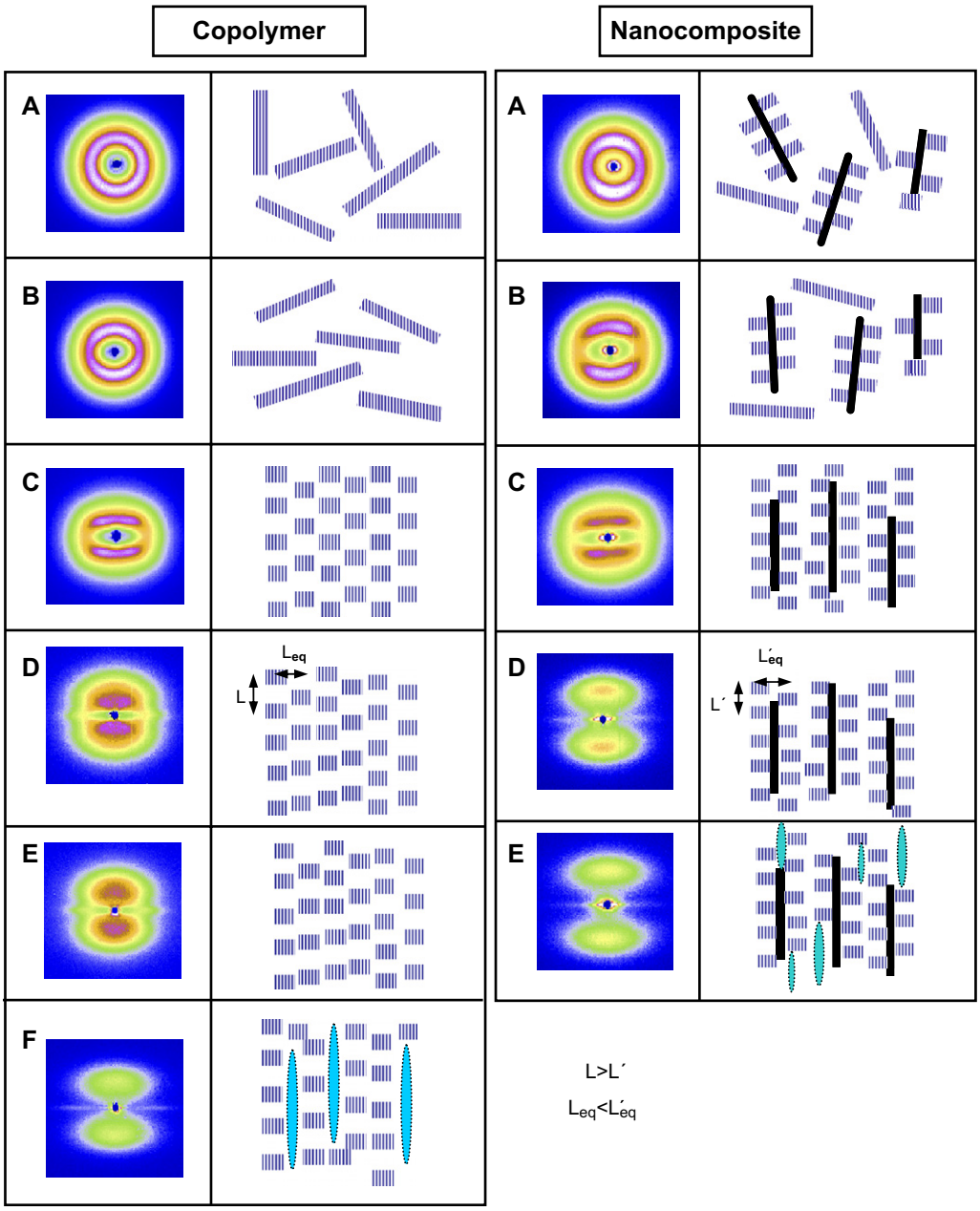

Fig. 8. 2D SAXS patterns together with the schemes of the corresponding microstructure, for the copolymer (left) and for the nanocomposite (right). The patterns have been chosen at following strains: A ≈ 0%, B ≈ 15%, C ≈ 35%, D ≈ 100%, E ≈ 135%, F ≈ 300%.

nanotubes and therefore the SAXS pattern, although presenting reminiscence of the four points pattern, reveals a higher degree of disorder. Secondly, at higher strains, the fragmented lamellae appear to reassemble themselves along the stretching direction interconnected by tie molecules, forming microfibrils. At this state, the SAXS patterns exhibit an equatorial streak with an intensity maximum (Fig. 4) related to the long period (L_{eq}) in the transverse direction (perpendicular to the applied stress) resulted from the average lateral distance between microfibrils. Such a long period increases with increasing strain for both copolymer and nanocomposite (Fig. 5). However, significantly higher values are measured for the nanocomposite at comparable strain. The appearance of such equatorial maxima upon stretching has been previously reported for PBT-*b*-PTMO copolymers [21,22] and the evolution with strain (Figs. 4 and 5) can be explained by the progressive destruction of the semicrystalline domains with increasing strain. Accordingly, our data indicate that this destruction is more efficient in nanocomposite than in copolymer. One possibility to visualize this fact is provided in the scheme of Fig. 8D, right. If one considers a fraction of the crystalline blocks anchored to the nanotubes then a strong restriction to the block displacement is expected. As a result, the stress can be more efficient in destroying the crystalline blocks. In some polymer composites with macroscopic fibres, the fibres can act as nucleating agents and promote transcrystallinity in an interphase region between the fibre and the bulk matrix. The effect of this transcrystalline layer on mechanical

properties appears to differ for different fibre/polymer systems [23,24]. In some cases it has been reported that the polymer nucleates in the rough areas of the fibre, and the anchored molecules thereby enhance the fibre–matrix adhesion through mechanical interlocking [25,26]. The last could be a similar effect to the one taking place at the present study. Thirdly, with a further increase in strain, the equatorial maxima tend to transform into an equatorial streak, as seen in Fig. 4 at strain 319% for copolymer and 94% for nanocomposite. This effect, previously observed in PBT-*b*-PTMO, was attributed to the formation of an elongated soft phase, referred to as soft needles [22], formed by the resulting material of the hard block destruction. The appearance of the soft needles precedes the mechanical failure of the material. Again, the appearance of an equatorial streak occurs for nanocomposite at smaller strain values than those for copolymer (Fig. 4). Therefore, analogously as in the previous step, we can assume that this fact occurs as a consequence of the anchoring of lamellae blocks to the nanotube surface (Fig. 8E, right). It should be noted that it is necessary to increase the strain, above 200%, in order to reach the final elongation of the soft phase in the copolymer (Fig. 8F).

5. Conclusions

The different mechanical behaviour between the PBT-*b*-PTMO block copolymer and its nanocomposite with 0.2 wt% of SWCNT can be correlated with the changes in microstructure during deformation.

For nanocomposite, the Young's modulus and the yield strength are higher than those of block copolymer, but the elongation-to-break is less than a half. The SWCNT can act as an anchor for the crystalline blocks in nanocomposite, sharing the applied load with PBT crystals and making the hard block destruction more efficient. This model explains the observed increase of the Young's modulus and the yield strength in the elastic region of the stress–strain curve, as well as the increase of the rigidity of nanocomposite, which shows a big decrease of the elongation-to-break in relation to the block copolymer.

Acknowledgements

The authors thank the financial support from the Spanish Ministry of Science and Education (Grant MAT2005-01768). M.C.G.G. and A.N. are also grateful to the Ramón y Cajal Program for the support of this research.

References

[1] Adams RK, Hoeschele GK. Thermoplastic polyester elastomers. In: Legge NR, Holden G, Schroeder HE, editors. Thermoplastic elastomers: a comprehensive review. Munich: Hanser Publishers; 1987.
[2] Baltá-Calleja FJ, Fakirov S, Roslaniec Z, Krumova M, Ezquerra TA, Rueda DR. J Macromol Sci Phys B 1998;37:219.
[3] Schroeder H, Cella RJ. Encyclopedia of polymer science and engineering, vol. 12. New York: John Wiley & Sons; 1988.
[4] Krishnan A, Dujardin E, Ebbesen TW, Yianilos PN, Treacy MMJ. Phys Rev B 1998;58:14013.
[5] Vaia RA, Wagner HD. Mater Today 2004;32:7.
[6] Brown MJ, Anderson DP, Justice RS, Lafdi K, Belfor M, Strong KL, et al. Polymer 2005;46:1054.
[7] Zhao C, Hu G, Justice R, Schaefer DW, Zhang S, Yang M, et al. Polymer 2005;46:5125.
[8] Hernández JJ, García-Gutiérrez MC, Nogales A, Rueda DR, Ezquerra TA. Compos Sci Technol 2006;66:2629.
[9] Rols S, Righi A, Alvarez L, Anglaret E, Almairac R, Journet C, et al. Eur Phys J B 2000;18:201.
[10] García-Gutiérrez MC, Nogales A, Rueda DR, Domingo C, García-Ramos JV, Broza G, et al. Polymer 2006;47:341.
[11] Salvetat JP, Andrew G, Briggs D, Bonard JM, Bacsa RR, Kulik AJ, et al. Phys Rev Lett 1999;82:944.
[12] Walters DA, Ericson LM, Casavant MJ, Liu J, Colbert DT, Smith KA, et al. Appl Phys Lett 1999;74:3803.
[13] Chen X, Burger C, Fang D, Sics I, Wang X, He W, et al. Macromolecules 2006;39:5427.
[14] Fakirov S, Fakirov C, Fischer EW, Stamm M. Polymer 1991;32:1173.
[15] Stribeck N, Sapoundjieva D, Denchev Z, Apostolov AA, Zachmann HG, Stamm M, et al. Macromolecules 1997;30:1329.
[16] Roslaniec Z, Broza G, Schulte K. Composite Interfaces 2003;10:95.
[17] Mencik Z. J Polym Sci Polym Phys 1975;13:2173.
[18] Guinier A. X-ray diffraction in crystals. In: Imperfect crystals and amorphous bodies. San Francisco: Freeman; 1963.
[19] Nogales A, Sics I, Ezquerra TA, Denchev Z, Baltá Calleja FJ, Hsiao BS. Macromolecules 2003;36:4827.
[20] García-Gutiérrez MC, Nogales A, Rueda DR, Domingo C, García-Ramos JV, Broza C, et al. Compos Sci Technol 2007;67:798.
[21] Stribeck N. J Polym Sci B Polym Phys 1999;37:975.
[22] Stribeck N. Analysis of SAXS fiber patterns by means of projections. In: Cebe P, Hsiao B, Lohse DJ, editors. Scattering from polymers, characterization by X-rays, neutrons and light. ACS symposium series, vol. 739. Oxford University Press; 2000 [chapter 3].
[23] Lustiger A. Polym Compos 1992;13:408.
[24] Dean DM, Marchione AA, Rebenfeld L, Register RA. Polym Adv Technol 1999;10:655.
[25] Wang C, Liu C-R. J Polym Sci B Polym Phys 1998;36:1361.
[26] Assouline E, Grigull S, Marom G, Wachtel E, Wagner HD. J Polym Sci B Polym Phys 2001;39:2016.